

Article

Controlling Atmospheric Corrosion of Weathering Steel Using Anodic Polarization Protection Technique

Hany S. Abdo , Asiful H. Seikh *, Ahmed Fouly  and Faraz H. Hashmi

Mechanical Engineering Department, King Saud University, P.O. Box 800, Al-Riyadh 11421, Saudi Arabia; habdo@ksu.edu.sa (H.S.A.); amohammed7.c@ksu.edu.sa (A.F.); 439106627@student.ksu.edu.sa (F.H.H.)

* Correspondence: aseikh@ksu.edu.sa

Abstract: The atmospheric corrosion of weathering steels varies as a function of geographic zone, season, and other environmental variables related to that region which the experiments have been done. Meanwhile, rusting is a continuous process, and it is the main corrosion product of atmospheric corrosion. The current study investigates the effects of rust on weathering steel in the localized region of Digha, a sea resort of West Bengal, India. The investigations have been performed by purposely accelerating the rusting of weathering steel in a laboratory within one week in order to simulate approximately 18 months of actual rusting that can be achieved at field exposure. Anodic polarization of weathering steel comparable to potentiostatic passivation is obtained by shorting weathering steel with nobler metals, such as copper or graphite. The effect of rust formation on corrosion resistance after being immersed in 0.01 M KCl solutions for polished and unpolished samples has been investigated using electrochemical techniques, such as potentiodynamic polarization and electrochemical impedance spectroscopy (EIS). The rusted surfaces' morphology and composition were characterized using field emission scanning electron microscope (FE-SEM) and energy dispersive X-ray analysis (EDX). Based on the obtained results, it is concluded that the progressive rusting of weathering steel leads to a decrease in corrosion rate.

Keywords: atmospheric corrosion; weathering steel; passivation; anodic polarization



Citation: Abdo, H.S.; Seikh, A.H.; Fouly, A.; Hashmi, F.H. Controlling Atmospheric Corrosion of Weathering Steel Using Anodic Polarization Protection Technique. *Processes* **2021**, *9*, 1469. <https://doi.org/10.3390/pr9081469>

Academic Editors: Eliane D'Elia and Ambrish Singh

Received: 15 July 2021

Accepted: 16 August 2021

Published: 23 August 2021

Publisher's Note: MDPI stays neutral with regard to jurisdictional claims in published maps and institutional affiliations.



Copyright: © 2021 by the authors. Licensee MDPI, Basel, Switzerland. This article is an open access article distributed under the terms and conditions of the Creative Commons Attribution (CC BY) license (<https://creativecommons.org/licenses/by/4.0/>).

1. Introduction

Corrosion of substances and materials that are exposed to open air and its pollutants, as opposed to submerged in fluid, is called atmospheric or air corrosion [1]. The ever-increasing dissatisfaction with atmospheric corrosion is leading in expense and weight loss of material above any other type of material degradation processes. Nevertheless, atmospheric corrosion is also accountable for half the corrosion damage every year [2]. However, some metals that form non-permeable layers give rise to the formation of oxides, which, in turn, achieve limited thickness through the dispersion of hardly noticeable oxide layers at room temperatures, unseen by the naked eye. In the case of metals such as chromium, titanium, and weathering steel, these limited thickness layers give an incredible shield over the metal surface.

Day-to-day enhancements in environmental contaminants have become a global concern. Different levels of pollutants entering the environment affect the corrosion rate. Few pollutants affecting the corrosion rate have been reported. Sulfur dioxide (SO₂) derived from the burning of petroleum products containing sulfur is estimated to be a leading factor in environmental corrosion [3,4]. The corrosion rates of non-coated metallic materials in the surrounding atmosphere are amplified by sulfur dioxide pollutants. Sulfur dioxide has higher dissolvability in water, giving rise to the formation of H₂SO₄ over the surface in the form of surface dampness thin layer [5,6]. Comparatively, levels of NO_x discharged from exhaust and combustion (street activities, traffic, and production of energy) are greater than emissions of sulfur dioxide [7,8]. Increasing environmental saltiness improves

the electrolyte arrangement of the surface by using hygroscopic salts (e.g., MgCl_2 and NaCl), which, in turn, enhance atmospheric corrosion rates. Several studies have stated that the core reason behind environmental corrosion is chloride ions [9–11]. Nonetheless, hydrogen peroxide (H_2O_2) is another pollutant available in the atmosphere, and it is the predisposition of hydrogen peroxide to be responsive to all iron alloys and composites, resulting in the production of HOX from its decomposition. Covering and steeping the surface of a target metal with a solution containing hydrogen peroxide results in the production of a passive layer [12,13]. Several studies [14,15] have revealed that most environmental changes and transformations of the atmosphere related to chlorinated hydrocarbons also contribute to fresh air purification levels.

Weathering steel (WS) comprises 1–2.5% alloying elements (Cr, Cu, Si, and P) and is the most common type of structural steel, widely used for bridges, buildings, etc. [16]. Moreover, it tends to form rust at a rate depending on the level of contact with oxygen in the presence of moisture and air. Researchers [17,18] demonstrated that the main products of environmental corrosion of steel are magnetite (Fe_3O_4), amorphous ferric oxy-hydroxide ($\text{FeO}_x(\text{OH})_{3-2x}$), and crystalline rust (α - FeOOH or γ - FeOOH) as well as β - FeOOH in marine environments. According to Kamimura et al. [18], corrosion begins with the anodic dissolution of iron into ferrous ions (Fe^{2+}). These ions react with the moisture (hydrolysis) on the surface of the steel to form FeOH^+ . The FeOH^+ , in turn, reacts with the oxygen (oxidation) in the atmosphere to form γ - FeOOH , which crystallizes and precipitates out of the system (the rate of crystallization and precipitation is increased if drying cycle occurs). Moisture mixed with pollutants such as sulfur dioxide (SO_2) has a relatively low pH. In contact with this mixture, the crystalline γ - FeOOH dissolves to form amorphous $\text{FeO}_x(\text{OH})_{3-2x}$, which precipitates again. Lastly, the $\text{FeO}_x(\text{OH})_{3-2x}$ undergoes a solid-state transformation (deprotonation hydroxyl ions from rainwater) to become α - FeOOH [19–21].

Using controlled passivation, the rust on weathering steel (WS), comparable to the rust formed on weathering steel due to a long period of exposure in Digha, was simulated. The simulation of the data was carried out by anodically polarizing the WS with a nobler metal, as the usage of a potentiostat would have been expensive and confined. Previous studies of Digha stated that 0.01 M KCl is found to be stable for simulating the data. Therefore, weathering steel was connected with nobler metals, such as Cu and graphite, and dipped in 0.01 M KCl. The corrosion rate of weathering steel that was anodically polarized with Cu or graphite showed a significant decrease in corrosion rate, confirming that the progressive rusting of weathering steel leads to a progressive decrease in the corrosion rate. The rust manufactured by this process was characterized by SEM and analyzed by EDX. The corrosion rate of WS obtained by this method was compared and rust characterized with data from 18-month field exposed WS in Digha. Thus, the study revealed that the protective layer of weathering that was produced after 18 months' exposure could easily be countered in the laboratory by connecting WS with nobler metals and dipping it in an appropriate solution. Using this inexpensive method, the corrosion rate of WS was also decreased.

Generally, this work aims to improve the atmospheric corrosion effect of commercial weathering steel in the localized region of Digha, a sea resort of West Bengal, India, using anodic polarization protection technique. The use of this technology ensures that the best anti-corrosion behavior of commercial weathering steel is obtained in the specified region, which has not been investigated before.

2. Experimental Procedure

2.1. Materials

For the present study, hot rolled weathering steel (WS) sheets (5 mm thick) sourced from a leading manufacturer was taken. The properties and chemical composition of WS are given in Table 1.

Table 1. Chemical composition and mechanical properties (yield strength YS and ultimate tensile strength UTS) of weathering steel.

Composition in Weight%								Mechanical Properties	
C	Si	Mn	P	S	Cr	Ni	Cu	YS (MPa)	UTS (MPa)
0.09	0.41	0.38	0.11	0.01	0.45	0.27	0.35	320	460

Microstructural characterization and surface morphology determination of the samples were carried out by field emission scanning electron microscopy (FE-SEM) using a JEOL-7600F, Tokyo, Japan, microscope. Elemental analysis was performed using energy dispersive X-Ray analysis (EDX), which connected to the abovementioned SEM device.

2.2. Electrochemical Corrosion Studies

The electrochemical corrosion studies were carried out on samples of dimensions 10×10 mm with 5 mm depth, which were cut from hot rolled weathering steel sheets. These samples were polished using various grades (500–1200 grades) of silicon carbide emery papers to get a smooth surface. An ultrasonic cleaner was then used to clean the specimens.

A three-electrode corrosion cell was used for EIS and potentiodynamic polarization measurements using a standard polarization cell test, in which a sample was taken as a working electrode; the graphite rod represented the auxiliary electrode, while standard calomel represented the reference electrode (SCE). Samples were mirror polished before each current transient experiment. The impedance experiments were performed using AC voltage 100 mV and a DC voltage of 1.0 V in the frequency range of 0.01 to 100 kHz [2,4,6]. The absolute impedance and phase angles were measured at each frequency, and Nyquist and Bode plots were obtained. Using actual and imaginary data components in a simplex fit model, the impedance data were fitted into a suitable equivalent electrical circuit. Based on this equivalent electrical circuit, the impedance data were analyzed. In this study, 0.01 M KCl at pH 8.8 solution was taken as the electrolyte for the corrosion test, while in some comparisons, 3.5% NaCl was used.

2.3. Rusting Procedure

Rusting of the samples in the laboratory was performed on polished as well as on weather exposed samples in 0.01 M KCl solution by two methods:

In the first set of experiments, weathering steel was connected with a nobler material (Cu or graphite) and dipped in a 0.01 M KCl solution until the polarized potential stabilized. The sample, in as received condition—i.e., in a rusted condition or in a polished condition—was connected with the nobler material (sample numbers SP1–SU4 of Table 2). It took 7 days to attain the stabilized potential and steady-state currents.

Table 2. Details of rusting by first method.

Sample Code	Condition	Connected in Solution W.R.T.	Electrolytes
SP1	Polished	Cu	0.01 M KCl
SP2	Polished	Graphite	0.01 M KCl
SU3	Unpolished	Cu	0.01 M KCl
SU4	Unpolished	Graphite	0.01 M KCl
SP5	Polished sample potentiodynamically polarized		0.01 M KCl
SU6	Unpolished Weather exposed sample potentiodynamically polarized		0.01 M KCl

3. Results and Discussions

3.1. Potentiodynamic Polarization Tests

From Table 3, it can be seen that when polished samples were shorted with copper or graphite, very low steady-state current values were obtained. Current transient data are given in Figure 1. Slightly higher current values were obtained with unpolished samples. However, steady-state polarized potentials are in the passive range, as can be seen from Figure 2. It is interesting to note that when current transient experiments were done by applying the same polarized potentials, the steady-state currents obtained were very close to those obtained in the first set of experiments performed with polished specimens (6 against 3.5 and 8 against 4.2 mA/cm², respectively). Thus, while it took 3600 s to attain 3.5 or 4.2 mA/cm² in the current transient experiment, it took 7 days to attain the steady-state currents in the first set of experiments where the steel samples were only shorted with copper/graphite and dipped in the solution. The effect in both the experiments was the same; the samples were both anodically polarized to the passive region of the steel. To cross check whether shorting the steel with nobler metal indeed gives the same effect as the passivation experiment done with the help of a potentiostat, weathering steel was shorted with nobler lead metal and dipped in a 0.01 KCl solution. The stabilized polarized potential and current was found to be 0.2 mV vs. SCE and 1.0 A/cm², respectively. When the current transient experiment of the same steel was carried out in 0.01 M KCl by subjecting it to a polarized potential of 0.2 mV vs. SCE, the steady-state current after 7 days was found to be 20.82 micro A/cm². This conclusively established the fact that shorting the steel with nobler metals gives the same effect as is obtained by anodic passivation by potentiostat. These experiments also confirmed that the progressive rusting of weathering steel led to a progressive decrease in corrosion rate.

Table 3. Current transient experiments.

Sample Code	Electrolyte	Stabilized Voltage (mV) vs. SCE	Stabilized Current (mA/cm ²)	Stabilized Voltage (mV) vs. SCE in Current Transient Curve *	Stabilized Current (mA/cm ²) in Current Transient Curve
SP1	0.01 M KCl	−607	44	−607	3.5
SP2	0.01 M KCl	−700	8	−700	4.2
SU3	0.01 M KCl	−586	6	−586	3.5
SU4	0.01 M KCl	−534	43	−534	3.7

* Current transient experiments were done on polished weathering steels by applying polarized potentials as indicated in the column.

Rust on weathering steel was also formed anodically using a standard potentiostat. Samples were polarized anodically in a potentiostat by applying polarized potential obtained from the first set of experiments. Incidentally, these potentials are in the passive range of the steel, as can be seen from Figure 2. Results of set 1 as well as current transient data are given in Table 3.

Corrosion rates of samples SP1–SU4 after the first set of experiments and samples SP5 and SU6 as per Table 2 in 0.01 M KCl solutions were measured by potentiodynamic polarization tests (Figure 2, Table 4). The corrosion rates of samples SP1–SU4 were also measured in 3.5% NaCl solution using a potentiodynamic polarization test (Figure 3, Table 5).

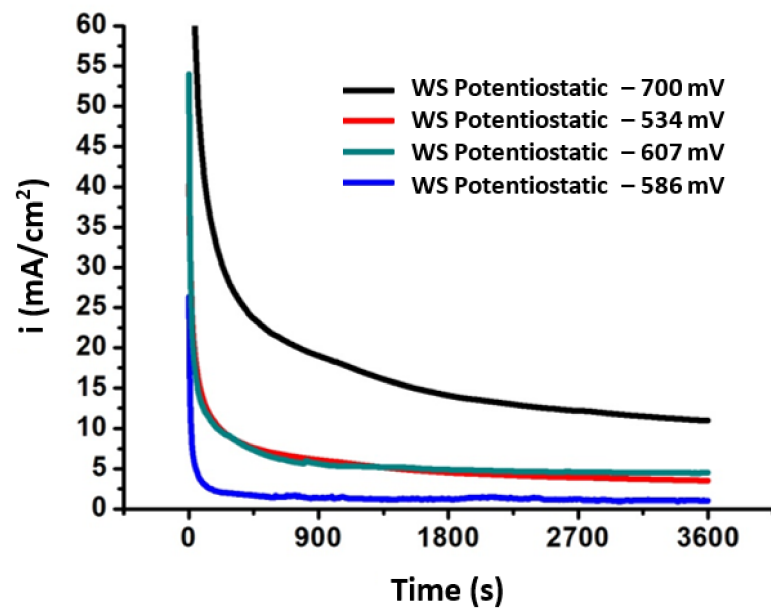


Figure 1. Current transients in 0.01 M KCl for different working sense (WS).

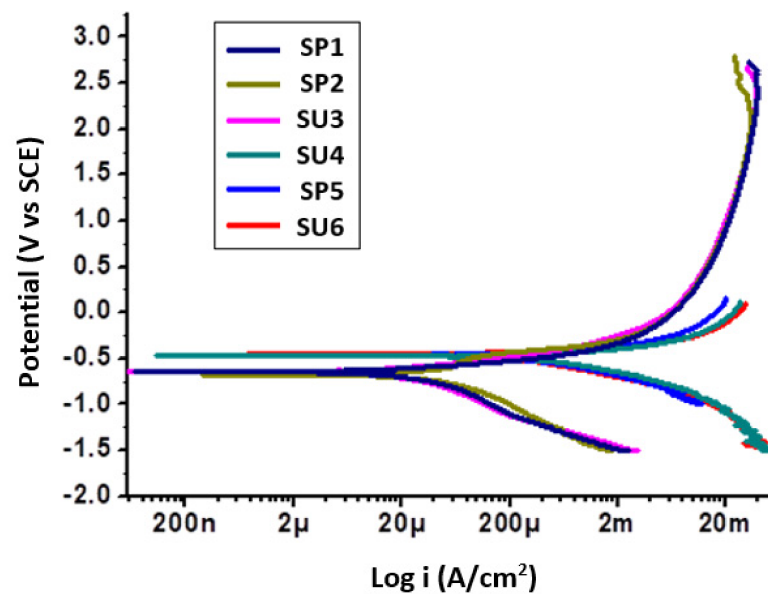


Figure 2. Potentiodynamic polarization diagram in 0.01 M KCl.

Table 4. I_{corr} and E_{corr} of Weathering Steel in 0.01 M KCl Solutions.

Sample Code	I_{corr} ($\mu\text{A}/\text{cm}^2$)	I_{corr} $\mu\text{m}/\text{yr}$	E_{corr} (mV) vs. SCE
SP1	15.88	19.50	-659.00
SP2	16.89	20.20	-456.20
SU3	16.30	21.50	-576.20
SU4	22.33	23.20	-588.20
SP5	26.26	30.66	-329.50
SU6	30.52	35.63	-512.90

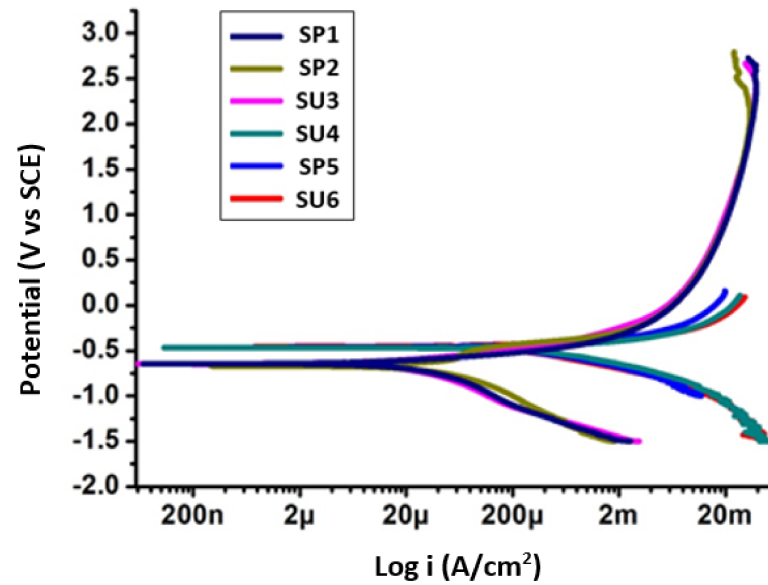


Figure 3. Potentiodynamic polarization diagram in 3.5% NaCl.

Table 5. I_{corr} and E_{corr} of weathering steel in 3.5% NaCl solutions.

Sample Code	I_{corr} ($\mu\text{A}/\text{cm}^2$)	E_{corr} (mV) vs. SCE
SP1	70.69	−910
SP2	109.7	−800
SU3	102.5	−1000
SU4	112.9	−788.2

From Figure 2, it can be seen that the potentiodynamic curve of samples SP1–SU4 almost merges with that of the weathering steel exposed in Digha. The I_{corr} values expressed in $\mu\text{A}/\text{cm}^2$ and $\mu\text{m}/\text{yr}$ as well as E_{corr} values are listed in Table 4. It can be noticed that the values corroborate the statement made above. The I_{corr} values expressed in $\mu\text{m}/\text{yr}$ show remarkable correlation with the corrosion rates of the field exposed corrosion rates given in Table 6. In fact, the corrosion rate of polished sample shorted with copper is almost same as that of the 24 months field exposed sample. It is interesting to note that, with increased exposure time, the corrosion rate decreased. From Table 4, it can also be inferred that shorting weathering steel with different nobler metals yields different corrosion rates. Therefore, corrosion rates similar to those of longer period field exposed samples can be obtained by shorting WS with other nobler metals or by exposing it beyond 7 days.

Table 6. Electrochemical impedance spectroscopy results of weathering steel.

Sample Code	R_u (ohm)	Y_0	α	Wd	R_p (ohm)
SP1	3.5×10^{-3}	1.125×10^{-6}	523×10^{-3}	12.61×10^{-3}	529.62
SP2	4.467×10^{-3}	1.329×10^{-9}	1	44.38×10^{-3}	336.25
SU3	5.6×10^{-3}	7.284×10^{-9}	859.5×10^{-3}	69.81×10^{-3}	502.00
SU4	44.82×10^{-6}	1.533×10^{-9}	1	6.588×10^{-3}	317.20
SP5	12.02×10^{-6}	16.63×10^{-9}	853.2×10^{-3}	249×10^{-3}	278.80
SU6	235.8×10^{-12}	24.16×10^{-10}	845.5×10^{-3}	65.98×10^{-3}	68.35

3.2. Electrochemical Impedance Spectroscopy (EIS)

From Figure 3 and Table 5, it can be seen that, while the unpolished sample shorted with copper gives the most active E_{corr} , the unpolished sample shorted with graphite gives

the most noble E_{corr} . Table 6 gives a comparative study of corrosion rates of weathering steel in 3.5% NaCl solution. Since the experimental corrosion rates in 3.5% NaCl solution also correlate well with the field exposed sample, it can be stated that a satisfactory simulation of 18-month Digha exposed rusting by shorting with copper was achieved.

A three-electrode corrosion cell was constructed using Auto Lab to generate electrochemical impedance spectroscopy measurements. Bode and Nyquist plots were obtained. In order to choose the respective models and to find the value of all fitting models, curve fitting was performed. A software installed on the instrument was used to calculate parameters including R_p , R_u , and Y_0 . Fit/simplex model program was used in order to fit the experimental data (Figures 4 and 5 and Table 6) in order to interpret impedance data (Figure 6) on the basis of an equivalent electric circuit (Figure 7). EIS was performed for a better understanding of the corrosion properties. The experiment was done for WS. All the EIS spectra complied with CPE with diffusion.

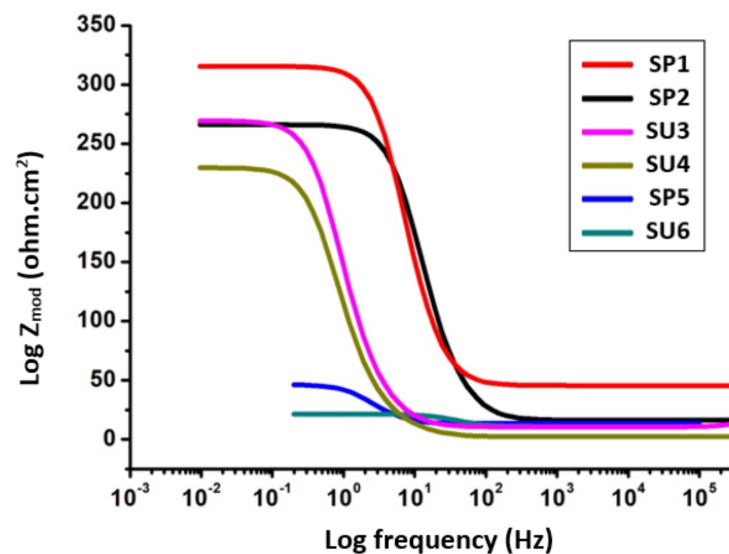


Figure 4. Bode plot (frequency-phase amplitude) in 0.01 KCl solution.

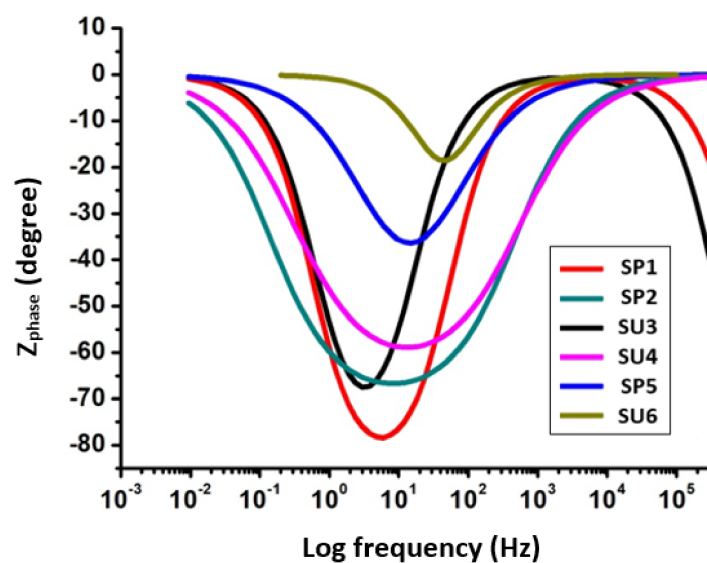


Figure 5. Bode plot (frequency-phase angle) in 0.01 M KCl solutions.

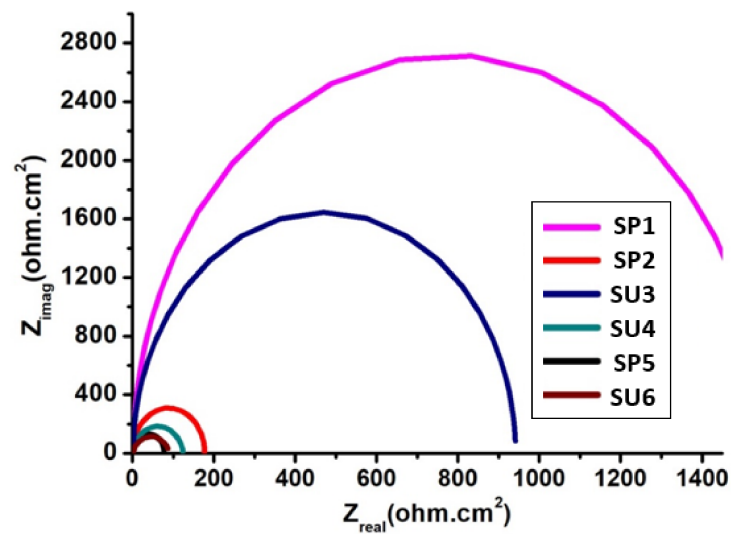


Figure 6. Nyquist plot in 0.01 M KCl.

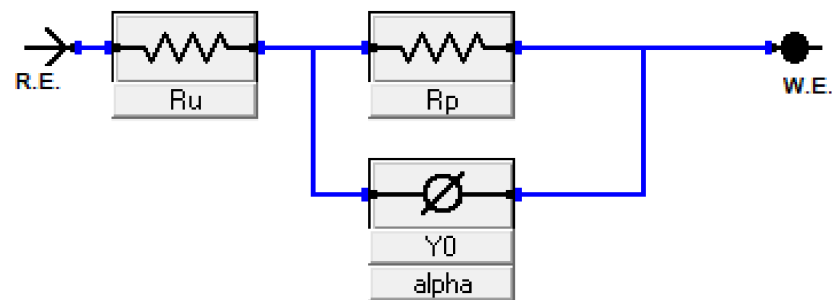


Figure 7. Equivalent circuit model.

3.3. Morphology and Surface Characterization

The morphology of the rust surface rusted potentiostatically when subjected to a constant potential of -607 mV vs. SCE and by forming a closed circuit with copper, which, as described earlier, was studied using field emission scanning electron microscopy (FE-SEM) and energy dispersive X-ray analysis (EDX). EDX analysis shows that the hematite (α - Fe_2O_3) represented the main corrosion product, which forms a protective layer against corrosion [22–26]. The micrographs and composition are given in Figures 8 and 9, respectively.

From Figures 2 and 3 and Table 6, it can be seen that, for sample SP1, the polarization resistance (R_p) is the highest ($R_p = 729$ ohm) and its corrosion rate is also lowest among all the samples. Similarly, the R_p is lowest for sample SU6 ($R_p = 68.35$ ohm) and its corrosion rate is high. Therefore, as the polarization resistance of the metal increases, the corrosion rate decreases. This is because an increase in polarization resistance means an increase in the thickness of the passive layer. Sample SP1 formed the most protective layer, so its resistance is high and hence its corrosion rate is at minimum. Sample SU6 is weather rusted, and its layer is not so well protected; therefore, its resistance is low, which is why its corrosion rate is high. Y_0 is inversely proportional to corrosion rate. It is highest for sample SP1 ($Y_0 = 1.125 \times 10^{-6}$) and lowest for sample SU6 (24.16×10^{-10}). All curves are fit using the CPE model. It is also seen from the Nyquist plot that all data have a single time constant. Sample SP1 had the largest diameter, so it has the lowest corrosion rate; sample SU6 has lowest polarization resistance. The modulus curves also show the same pattern. Sample SP1 behaves like capacitance as its angle is approximately 90° , and sample SP1 acts as a resistor, as its angle is close to 0° .

SEM and EDX analysis were performed for rust morphology studies of the steels passivated by potentiostat as well as by the method of dipping samples in a solution and connecting them to nobler metals. From Figures 8 and 9, it is seen that, in both cases, the rust morphology and composition were of a globular, non-compact type and correlated with field exposed rust.

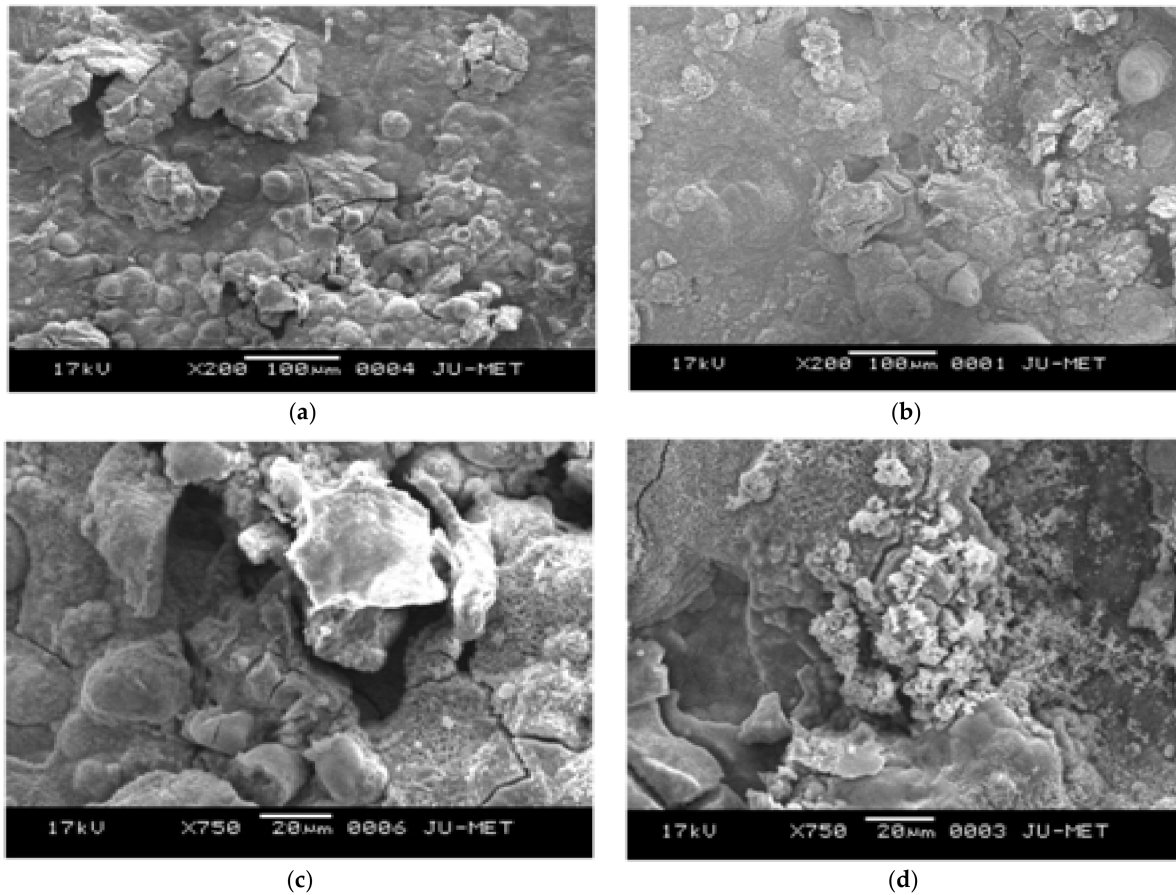


Figure 8. SEM image of: (a,b) rusting at -607 mV by potentiostat, (c,d) rusting by connecting with copper.

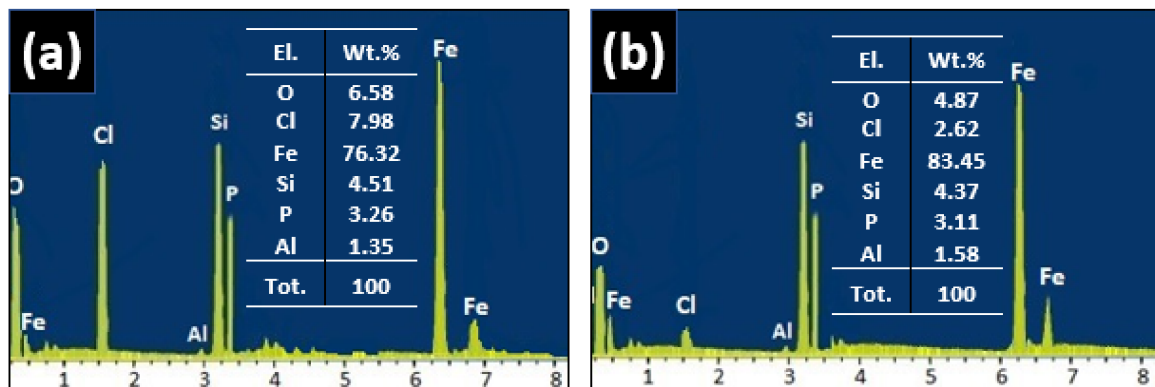


Figure 9. EDX elemental analysis of: (a) rusting at -607 mV by potentiostat, (b) rusting by connecting with Copper.

4. Conclusions

Weathering steel was connected with nobler metals in order to simulate the production of rust that can occur during long periods of exposure in Digha, a sea resort of West Bengal, India. The following qualitative and quantitative conclusions can be made:

1. Anodic passivation of weathering steel comparable to potentiostatic passivation is obtained by shorting weathering steel with nobler metals (copper or graphite). However, the lower corrosion rate of the weathering steel further revealed that, besides the progressive rusting of weathering steel, other factors such as the binding force between the rust and the substrate also affect the corrosion rate significantly.
2. A simulation of 18 months field exposed weathering steel in Digha is achieved by shorting weathering steel with copper and dipping it in 0.01 M KCl solutions. Meanwhile, from SEM images and EDX analysis, the morphology of the rust obtained by two weeks' laboratory simulation correlates well with the rust obtained in 18-month field exposed samples.
3. The corrosion rate of weathering steel that was anodically polarized with Cu or graphite showed a significant decrease in corrosion rate, confirming that the progressive rusting of weathering steel leads to a progressive decrease in corrosion rate. Specifically, anodic polarization using copper increased the corrosion resistance by 80 and 89% for the polished and unpolished samples, respectively; using graphite in polarization increased the corrosion resistance by only 13.6 and 20% for the polished and unpolished samples, respectively.
4. From the EDX analysis of the rust layer, the main corrosion product of iron oxide (hematite α -Fe₂O₃) represents a very beneficial protective layer initiated by the mechanism of chemical interaction between the exposed steel surface and the solution intensified by the formation of micro galvanic pairs, which reduce the corrosion rate.

Author Contributions: Conceptualization, H.S.A. and A.H.S.; Data curation, A.F. and F.H.H.; Formal analysis, A.H.S. and A.F.; Funding acquisition, A.H.S.; Investigation, H.S.A.; Methodology, H.S.A., A.H.S. and A.F.; Resources, A.H.S.; Software, H.S.A.; Supervision, H.S.A.; Validation, F.H.H.; Writing—original draft, H.S.A. and A.H.S.; Writing—review & editing, H.S.A. All authors have read and agreed to the published version of the manuscript.

Funding: This research is funded by Researchers Supporting Project (number RSP-2021/373), King Saud University, Riyadh, Saudi Arabia.

Institutional Review Board Statement: Not applicable.

Informed Consent Statement: Not applicable.

Data Availability Statement: Not applicable.

Acknowledgments: The authors would like to acknowledge the Researchers Supporting Project (number RSP-2021/373), King Saud University, Riyadh, Saudi Arabia.

Conflicts of Interest: The authors declare no conflict of interest.

References

1. Craig, B.; Pohlman, S.L. Metals handbook, ninth edition: Volume 13—Corrosion (ASM Handbook). In *ASM Metals Handbook*; ASM International: Russell Township, OH, USA, 1987; pp. 80–83; ISBN 978-0871700193.
2. Abdo, H.S.; Seikh, A.H.; Mandal, B.B.; Mohammed, J.A.; Ragab, S.A.; Abdo, M.S. Microstructural Characterization and Corrosion-Resistance Behavior of Dual-Phase Steels Compared to Conventional Rebar. *Crystals* **2020**, *10*, 1068. [[CrossRef](#)]
3. Shreir, L.L.; Jarman, R.A.; Bursten, G.T. Corrosion Metal—Environment Reactions. In *Corrosion*; Butterworth Heinemann: Oxford, UK, 1994; Volume 1, p. 22; ISBN 0-7506-1077-8.
4. Abdo, H.S.; Abdus Samad, U.; Mohammed, J.A.; Ragab, S.A.; Seikh, A.H. Mitigating Corrosion Effects of Ti-48Al-2Cr-2Nb Alloy Fabricated via Electron Beam Melting (EBM) Technique by Regulating the Immersion Conditions. *Crystals* **2021**, *11*, 889. [[CrossRef](#)]
5. Barton, K. *Protection against Atmospheric Corrosion: Theories and Methods*; Wiley: New York, NY, USA, 1976; ISBN 0471013498.

6. Abdo, H.S.; Seikh, A.H.; Mohammed, J.A.; Uzzaman, T. Ameliorative Corrosion Resistance and Microstructure Characterization of 2205 Duplex Stainless Steel by Regulating the Parameters of Pulsed Nd:YAG Laser Beam Welding. *Metals* **2021**, *11*, 1206. [[CrossRef](#)]
7. Seinfeld, J. *Atmospheric Chemistry and Physics of Air Pollution*; Wiley: New York, NY, USA, 1986.
8. Sundaram, M.; Mohan, P.S.; Ananth, V. Metallic corrosion. In Proceeding of the 10th International Congress on Metallic Corrosion, Madras, India, 7–11 November 1987; pp. 143–146.
9. Rodríguez, J.J.S.; Hernández, F.J.S.; González, J.E.G. The effect of environmental and meteorological variables on atmospheric corrosion of carbon steel, copper, zinc and aluminium in a limited geographic zone with different types of environment. *Corros. Sci.* **2003**, *45*, 799–815. [[CrossRef](#)]
10. Abdo, H.S.; Sarkar, A.; Gupta, M.; Sahoo, S.; Mohammed, J.A.; Ragab, S.A.; Seikh, A.H. Low-Cost High-Performance SnO₂-Cu Electrodes for Use in Direct Ethanol Fuel Cells. *Crystals* **2021**, *11*, 55. [[CrossRef](#)]
11. De Meybaum, B.R.; Ayllon, E.S. Characterization of Atmospheric Corrosion Products on Weathering Steels. *Corrosion* **1978**, *36*, 1139–1151. [[CrossRef](#)]
12. Santana Rodríguez, J.J.; Santana Hernández, F.J.; González González, J.E. Mathematical and electro-chemical characterisation of the layer of corrosion products on carbon steel in various environments. *Corros. Sci.* **2002**, *44*, 2597–2610. [[CrossRef](#)]
13. Wang, J.H.; Wei, F.I.; Chang, Y.S.; Shih, H.C. The corrosion mechanisms of carbon steel and weathering steel in SO₂ polluted atmospheres. *Mater. Chem. Phys.* **1997**, *47*, 1–8. [[CrossRef](#)]
14. Misawa, T.; Asami, K.; Hashimoto, K.; Shimodaira, S. The mechanism of atmospheric rusting and the protective amorphous rust on low alloy steel. *Corros. Sci.* **1974**, *14*, 279–289. [[CrossRef](#)]
15. Yamashita, M.; Miyuki, H.; Matsuda, Y.; Nagano, H.; Misawa, T. The long term growth of the protective rust layer formed on weathering steel by atmospheric corrosion during a quarter of a century. *Corros. Sci.* **1994**, *36*, 283–299. [[CrossRef](#)]
16. Feliu, S.; Morcillo, M.; Feliu, S. The prediction of atmospheric corrosion from meteorological and pollution parameters-II. Long-term forecasts. *Corros. Sci.* **1993**, *34*, 415–422. [[CrossRef](#)]
17. Abdo, H.S.; Seikh, A.H.; Mohammed, J.A.; Luqman, M.; Ragab, S.A.; Almotairy, S.M. Influence of Chloride Ions on Electrochemical Corrosion Behavior of Dual-Phase Steel over Conventional Rebar in Pore Solution. *Appl. Sci.* **2020**, *10*, 4568. [[CrossRef](#)]
18. Kamimura, T.; Hara, S.; Miyuki, H.; Yamashita, M.; Uchida, H. Composition and protective ability of rust layer formed on weathering steel exposed to various environments. *Corros. Sci.* **2006**, *48*, 2799–2812. [[CrossRef](#)]
19. Samosir, R.; Simanjuntak, S.L. The influence of concentration and pH on corrosion rate in stainless steels—316 solution HNO₃ medium. In *IOP Conference Series: Materials Science and Engineering*; IOP Publishing: Bristol, UK, 2017; Volume 237, p. 012047. [[CrossRef](#)]
20. Alodan, M.A. Modeling of pH Distribution over Corrosion Sites. *J. King Saud Univ. Eng. Sci.* **2003**, *15*, 1–11. [[CrossRef](#)]
21. Rozali, A.A.; Masdek, N.R.N.; Murad, M.C.; Salleh, Z.; Hyie, K.M. The Effect of pH Value on the Corrosion Behaviour of Ti-6Al-4V and 316L SS Alloys under Physiological Environment. *Chem. Eng. Trans.* **2018**, *63*, 769–774. [[CrossRef](#)]
22. Pettersson, J.; Asteman, H.; Svensson, J.E.; Johansson, L.G. KCl Induced Corrosion of a 304-type Austenitic Stainless Steel at 600 °C; The Role of Potassium. *Oxid. Met.* **2005**, *64*, 23–41. [[CrossRef](#)]
23. Jonsson, T.; Froitzheim, J.; Pettersson, J.; Svensson, J.E.; Johansson, L.G.; Halvarsson, M. The Influence of KCl on the Corrosion of an Austenitic Stainless Steel (304L) in Oxidizing Humid Conditions at 600 °C: A Microstructural Study. *Oxid. Met.* **2009**, *72*, 213–239. [[CrossRef](#)]
24. Sim, J.H.; Kim, Y.S.; Cho, I.J. Corrosion behavior induced by LiCl-KCl in type 304 and 316 stainless steel and copper at low temperature. *Nucl. Eng. Technol.* **2017**, *49*, 769–775. [[CrossRef](#)]
25. Larsson, E.; Gruber, H.; Hellström, K.; Jonsson, T.; Liske, J.; Svensson, J.E. A Comparative Study of the Initial Corrosion of KCl and PbCl₂ on a Low-Alloyed Steel. *Oxid. Met.* **2017**, *87*, 779–787. [[CrossRef](#)]
26. Malede, Y.C.; Montgomery, M.; Dahl, K.V.; Hald, J. Effect of microstructure on KCl corrosion attack of modified AISI 310 steel. *Mater. High Temp.* **2018**, *35*, 243–254. [[CrossRef](#)]